Lab on a Chip

ROYAL SOCIETY OF CHEMISTRY

PAPER

View Article Online
View Journal

Cite this: DOI: 10.1039/d6lc00339g

Light-guiding capillaries: a robust optofluidic platform for nanoparticle tracking analysis

Torsten Wieduwilt,[a] Matthias Zeisberger,[a] Walter Hauswald,[a] Adrian Lorenz,[a] Shayan Vazirieh Lenjani,[b] Christian Rossner[bcd] and Markus A. Schmidt*[aef]

Received 22nd April 2026,
Accepted 26th May 2026

DOI: 10.1039/d6lc00339g

rsc.li/loc

Understanding nanoparticle interactions at the nanoscale is essential for numerous scientific fields and applications, with waveguide-based approaches offering a promising solution. In this work, we present a fiber-integrated platform for nanoparticle tracking analysis based on a fiber-type capillary structure (hereinafter referred to as "capillary") that achieves high performance comparable to more complex microstructured fibers. By combining measurements with optical simulations, we validate light propagation and loss behavior in water-filled capillaries, showing excellent agreement with theoretical predictions. The capillary-based approach provides structural simplicity, robustness, and compatibility with fiber systems, while enabling diffraction-limited imaging and accurate determination of hydrodynamic diameters for mono- and polydisperse nanoparticle ensembles. The demonstrated platform may serve as a future foundation for the characterization of nanoscale species in confined geometries and could be relevant for applications in nanoscience, bioanalytics, and environmental analysis.

1 Introduction

Nanoparticle tracking analysis (NTA) works by recording trajectories of individual diffusing nano-objects using image-based tracking and analyzing them *via* mean square displacement (MSD) analysis. Applying the Einstein–Stokes relation, the hydrodynamic diameter of each nanoparticle (NP) can be derived from its diffusion coefficient. This technology makes it possible to characterize small NP concentrations and polydisperse samples.

In addition to the NTA method, a range of diffusion-based techniques have been developed to determine the hydrodynamic diameter of NPs, which can be broadly divided into two groups: (i) approaches that require fluorescent labeling, such as microfluidic diffusional sizing (MDS),[1] nanofluidic diffusional sizing (NDS)[2] and fluorescence correlation spectroscopy (FCS),[3] and (ii) label-free techniques, including dynamic light scattering (DLS),[4] interferometric scattering microscopy (iSCAT)[5] and Taylor dispersion analysis (TDA)[6,7] (see SI, sec. S1 for details).

One promising NTA approach introduced in recent years is fiber-assisted NTA (FaNTA).[8] Here NPs diffusing in a liquid-filled microchannel along an optical fiber are illuminated by the modal field and the trajectories are obtained from the sidewise scattered light. In addition to fast imaging and compatibility with fiber and microfluidic systems, FaNTA's key advantage is the confinement of diffusing NPs within the illuminated volume and focal plane, enabling exceptionally long trajectories of fast-diffusing objects and highly accurate size determination.

Various FaNTA-related experiments have been reported, including 3D tracking in modified step-index fibers,[9] or the observation of previously unknown optical modes.[10] A particularly promising approach involves fibers with anti-resonant elements, enabling core diameters in the tens of micrometers range. This reduces confinement effects and enables the parallel tracking of hundreds of NPs.

In addition to hollow-core fibers,[11] the current state-of-the-art FaNTA platform is based on fibers with a single anti-resonant element (1-ARE). Here, light is guided inside a thin glass annulus attached to the inner wall of a support capillary. This platform has been used to assess the polydispersity of polystyrene nanoparticles[12] and to track gold nanoparticles as small as 9 nm.[13] The concept has also been extended to nanoprinted hollow-core waveguides on silicon chips[14] and fiber end faces.[15]

---

[a] Leibniz Institute of Photonic Technology, Albert-Einstein-Str. 9, 07745 Jena, Germany. E-mail: markus-alexander.schmidt@uni-jena.de
[b] Leibniz Institute of Polymer Research Dresden, Hohe Straße 6, 01069 Dresden, Germany
[c] Faculty of Chemistry and Food Chemistry, Technische Universität Dresden, Bergstrasse 6, 01069 Dresden, Germany
[d] Department of Polymers, University of Chemistry and Technology Prague, Technická 5, 16628 Prague 6, Czech Republic
[e] Otto Schott Institute of Material Research, Friedrich Schiller University Jena, Fraunhoferstr. 6, 07743 Jena, Germany
[f] Abbe Center of Photonics and Faculty of Physics, Friedrich Schiller University of Jena, Max-Wien-Platz 1, Jena 07743, Germany

Despite their effectiveness, 1-ARE fibers have several limitations, including complex fabrication to achieve homogeneous membrane thicknesses over extended lengths, the need for precise geometric alignment during measurements, and degraded optical imaging caused by multiple curved interfaces in the microscopic path.

A promising alternative are single-interface capillaries, which represent a concentric arrangement of a low-index circular channel (core) surrounded by an infinitely extended high-index medium. As the simplest form of microstructured fiber, capillaries are straightforward to fabricate, offer perfect azimuthal symmetry, and minimize the number of transverse interfaces – favorable properties for NTA. Note that since light guidance in capillaries is governed by Fresnel reflection, they exhibit higher losses than anti-resonant hollow-core fibers, which principally can be mitigated by inner-wall coatings.[16]

In this work, we investigate the use of fiber-type capillaries for waveguide-based NTA by combining optical simulations, loss measurements, and particle tracking experiments on gold and polystyrene NP ensembles (Fig. 1).

We characterize modal losses in water-filled capillaries, evaluate imaging performance through ray-tracing simulations, and demonstrate particle tracking using an image-based analysis workflow. The results are benchmarked against microstructured fibers (1-ARE fibers), to assess the performance of the capillary platform.

2 Results and discussion

2.1 Concept

Light guidance in a single-interface capillary structure is governed by Fresnel reflection at the channel boundary. Due to the lower refractive index of the channel (core), a portion of the light is transmitted through the interface (channel wall), resulting in modal losses. In the large-core limit ($r_c \gg \lambda_0$, r_c: core radius, λ_0: operation wavelength) mode formation is well described by the Marcatili–Schmeltzer model[17] or by the model presented in ref. 18. The latter (see SI, sec. S2) provides the following expressions for the loss of the various modes in a water-filled silica capillary, depending on the core radius r_c [cm] at a wavelength of 532 nm:

$$\gamma\left[\mathrm{dB\ cm^{-1}}\right] = \frac{1}{r_c{}^3}\cdot\begin{cases} 7.878\times10^{-10}\ \mathrm{cm}^2\cdot j_{1,n}^2 & :\mathrm{TE}_{0n} \\ 9.426\times10^{-10}\ \mathrm{cm}^2\cdot j_{1,n}^2 & :\mathrm{TM}_{0n} \\ 8.652\times10^{-10}\ \mathrm{cm}^2\cdot j_{m-1,n}^2 & :\mathrm{HE}_{mn} \\ 8.652\times10^{-10}\ \mathrm{cm}^2\cdot j_{m+1,n}^2 & :\mathrm{EH}_{mn} \end{cases} \tag{1}$$

Here, j_{mn} stands for the n-th root of Bessel function J_m. Particularly noteworthy is the $1/r_c{}^3$ dependence, which clearly indicates that increasing the core size reduces modal losses. Another key feature is the absence of resonances, enabling capillary operation across a continuous wavelength range, unlike anti-resonant waveguides, where structural interference in the membranes leads to alternating spectral domains of high and low transmission.

Using experimentally relevant parameters (λ_0 = 532 nm, n_{water} (20 °C, 532 nm) = 1.3354,[19] n_{silica} (532 nm) = 1.4607 (ref. 20)), eqn (1) predicts losses for the fundamental HE$_{11}$ mode in a water-filled capillary of 2.6 dB cm^{-1} $< \gamma <$ 11.9 dB cm^{-1} for microchannel diameters 25 μm $> d_c >$ 15 μm (Fig. 2).

These values are significantly higher than those of comparable annular structures (*e.g.* 1-ARE fibers). Notably, higher-order modes exhibit substantially greater losses, highlighting the relevance of the fundamental mode.

The NTA experiments involve recording the diffusive motion of a NP ensemble in water by microscopically imaging the laterally scattered light and statistically analyzing

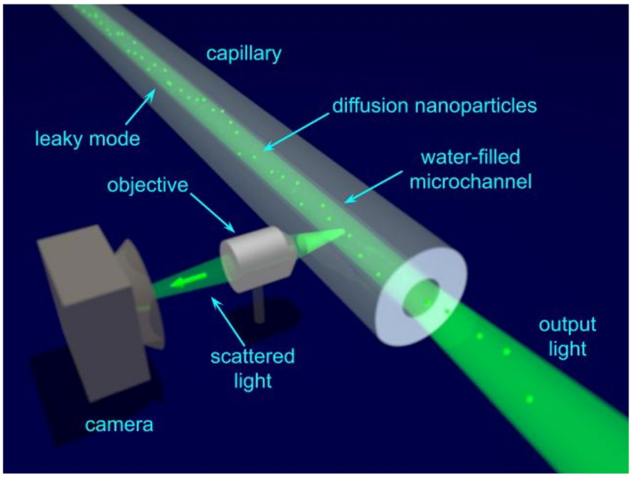

Fig. 1 Illustration of light guidance in a water-filled capillary used for nanoparticle tracking analysis (green: guided light, bright green: diffusing nanoparticles, light gray: capillary).

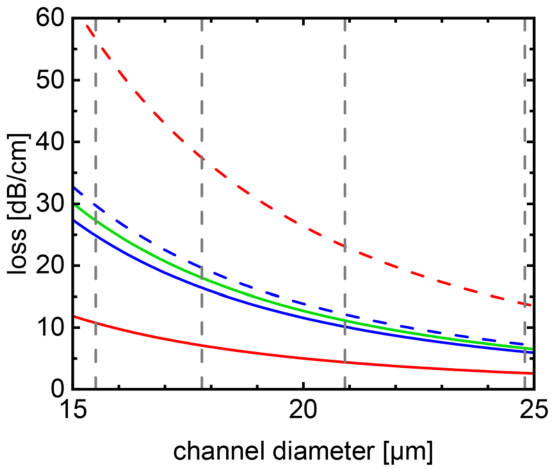

Fig. 2 Simulation of the modal loss as a function of the channel diameter of different modes in a water-filled silica capillary (λ_0 = 532 nm). The different colors refer to different modes (red-solid: HE$_{11}$, red-dashed: HE$_{12}$, green-solid: HE$_{21}$, blue-solid: TE$_{01}$, blue-dashed: TM$_{01}$). The gray-dashed vertical lines indicate the experimentally relevant core diameters used in our study.

the individual trajectories using mean-square displacement (MSD) analysis. The diffusion coefficient D of each NP is extracted from the slope of its MSD curve and converted into the hydrodynamic diameter d_h using the Stokes–Einstein relation, taking into account the viscosity of water[21] (see SI, sec. S3). The mean hydrodynamic diameter of the ensemble is computed by weighting each hydrodynamic diameter by its trajectory length (unit: frames) and dividing the sum of all weighted diameters by the total number of frames across all trajectories. In addition, the coefficient of variation ($\mathrm{CV} = \sigma/\mu$, with σ as the standard deviation and μ as the mean value) is calculated to quantify the precision of this statistically limited measurement method. Trajectories were extracted using the Python package Trackpy (see SI, sec. S4). Note that the accuracy of the diffusion coefficient obtained from MSD analysis increases with the number of frames per trajectory.[12] To further enhance the statistical significance of the results, complex data processing was performed, including z-score filtering and corrections for the effect of transversely restricted diffusion (see sec. S4 of the SI).

2.2 Results

To validate the theoretically predicted losses, we performed experimental measurements on capillaries filled with ultrapure water, featuring channel diameters of 15.5, 17.8, 20.9, and 24.8 μm (Fig. 2). Using a previously reported FaNTA setup[12,13,22] comprising a 532 nm laser (Coherent Verdi G), a polarization controller, a microscope with tubus lens, and camera (Fig. 3(a)), we recorded the intensity of side-scattered light at different axial positions along the capillary. Light was launched into the capillary *via* a butt-coupled homemade delivery fiber (NA = 0.05, mode field diameter: 8.5 μm). To enhance the scattered light collected by the microscope, the input light was linearly polarized perpendicular to the optical axis using a manual two-paddle fiber polarization controller. Scattered light from the capillary's fluidic channel was imaged using an Olympus Plan N 10 × 0.25 infinity-corrected objective. The field of view along the capillary axis was 1.41 mm. Imaging was performed with a CMOS camera (Basler acA4096-40um) featuring a (4096 × 2168) pixel sensor with a pixel size of (3.45 × 3.45) μm. For mechanical stabilization and background suppression, the capillary was mounted on a polished fused silica block placed on a xyz-translation stage. To reduce aberrations from the capillary's curved surface, a 0.4 mm-thick fused silica cover slip was placed over the imaged region, and the gap between capillary and cover slip was filled with index-matching liquid (n_D (20 °C) = 1.458). To maintain parallel alignment of the cover slip with the block, two identical capillaries were placed adjacent to the central one (see Fig. 3(b)).

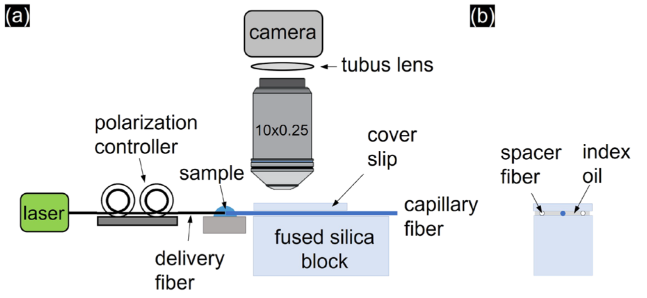

Fig. 3 Schematic of the experimental setup. (a) Side view showing the position of the objective relative to the capillary. (b) Front view of the glass block with the capillary and two spacer fibers beneath the cover slip.

Losses were determined by measuring the side-scattered light along the water-filled capillary over a distance of (8–10) mm, with the fiber translated under the microscope in 1 mm steps. To achieve sufficient signal intensity, an exposure time of 1 s was used with a laser power of 120 mW at the butt-coupling interface. As an example of the measurement results, Fig. 4 shows selected images of the sidewise emitted light from a capillary with a channel diameter of d_c = 17.8 μm recorded at different longitudinal positions. A clear decrease in intensity with increasing distance from the capillary entrance is observed, reflecting the transmission losses due to Fresnel reflection at the core-cladding interface.

Based on these images, the longitudinal intensity profile along the center of the water-filled core – *i.e.*, the middle of the bright regions of the images – was extracted. Fig. 5(a) displays the combined profiles, with each color corresponding to data from a single image, clearly showing a decrease in intensity with increasing distance from the capillary input. Note that as the step size (1 mm is smaller than the captured image length (1.41 mm), the intensity profiles partially overlap. A linear curve (white line in Fig. 5(a)) was applied to the data, and the resulting slope was used to determine the modal loss.

Using this procedure, the loss of four selected capillaries with different channel diameters (Table 1) were determined and compared with theoretical predictions (Fig. 5(b)). The experimental results show excellent agreement with the theoretical curve, confirming both the validity of the model and the high quality of the fabricated capillaries. The slightly elevated measured values may be caused by the excitation of higher-order modes, which exhibit greater losses (Fig. 2).

Fig. 4 Examples of microscopic images showing side-scattered light from a water-filled silica capillary with an inner channel diameter of d_c = 17.8 μm (λ_0 = 532 nm). Each image represents a 1.41 mm-long section along the capillary. The eight images are vertically stacked, with the total distance from the capillary entrance indicated by the labels on the left.

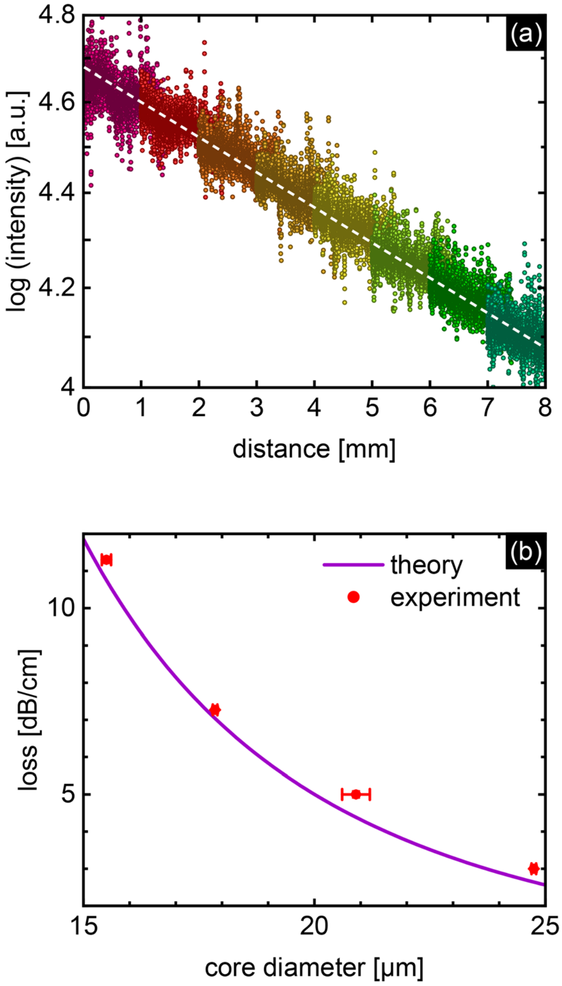

Fig. 5 (a) Intensity distribution of side-scattered light from a water-filled capillary (d_c = 17.8 μm, capillary B) along a total length of 8 mm, resulting from evaluating the images shown in Fig. 4 each color represents a different distance from the capillary input (*cf.* Fig. 4). The dashed white line indicates the slope corresponding to modal loss. (b) Comparison of theoretically (solid line) and experimentally (red points) determined modal loss of water-filled capillaries as a function of channel diameter in the range of 15 μm < d_c < 25 μm.

It is important to note that slight periodic intensity modulations are observed in capillaries with large channel diameter, caused by weak excitation of the HE_{12} higher-order mode and the resulting beating with the fundamental mode. This excitation arises from the mismatch between the Bessel-like mode profile of the capillary and the Gaussian mode of the delivery fiber (more details in SI, sec. S6). The resulting interference leads to periodic intensity variations along the capillary, which, however, are practically negligible due to the high loss of the HE_{12} mode. The exposure time used in the loss experiments are about 500 times longer than in the actual NTA experiments, making the contribution of light scattered by the water negligible in the NTA measurements.

2.3 Applications

To demonstrate the suitability of capillaries (Fig. 6(a)) for NTA, several FaNTA experiments were conducted on a well-characterized ensemble of ultra-uniform nanospheres in aqueous solution and compared with results obtained using a 1-ARE fiber (Fig. 6(b)), starting with the characterization of a monodisperse solution of gold nanospheres.

Monodisperse solution of gold nanospheres. The choosen NPs (nanoComposix) have a manufacturer-specified physical diameter of (28 ± 0.9) nm (TEM) and a hydrodynamic diameter of d_h = 36 nm, due to the functionalization of the nanoparticle surface with lipoic-dPEG$_{12}$–COOH ligands, that forming an electric double layer. The coefficient of variation CV for the physical diameter, based on TEM data, is specified as CV = 0.031. Note that the NP ensemble exhibits a very low polydispersity index of 0.01 and can therefore be classified as monodisperse.[23] To ensure a statistically meaningful number of NPs within the observation volume - defined by the channel diameter (capillary: d_c = 16 μm; 1-ARE fiber: d_c = 16.6 μm) and the camera image length (1.41 mm) – the stock solution (2.4 × 10^{11}) NPs ml^{-1} was diluted 2350-fold using ultra-pure water containing 2 mM sodium citrate. The sodium citrate serves to prevent nanoparticle aggregation during measurements.

A water-filled capillary with a channel diameter of d_c = 16 μm ($\gamma \approx 10$ dB cm^{-1} at λ_0 = 532 nm) was selected for the FaNTA experiments (Fig. 2 and 6(a)). This diameter was chosen to match the depth of field of the microscope objective (Olympus Plan N 10 × 0.25) used for particle detection, avoiding deterioration in image quality when the NP approaches the top or bottom of the microchannel. For comparison, the selected 1-ARE fiber featured a channel diameter of d_c = 16.6 μm (Fig. 6(b)), closely matching that of the capillary. Note that a membrane thickness of 700 nm was chosen for the ARE to ensure low-loss guidance at λ_0 when the fiber is filled with water. The choice of the comparably short excitation wavelength of λ_0 = 532 nm is optimal for 28 nm gold NPs due to the plasmonically enhanced scattering

Table 1 Comparison of theoretically and experimentally determined loss for four water-filled silica capillaries at λ_0 = 532 nm. Channel diameters were measured by SEM, with the measurement uncertainty defining the error margins. Capillary C exhibits a slightly elliptical channel geometry, leading to an increased diameter tolerance

Parameter	Capillary A	Capillary B	Capillary C	Capillary D
Core diameter [μm], SEM	15.5 ± 0.1	17.8 ± 0.05	20.9 ± 0.3	24.8 ± 0.05
Loss (theory) [dB cm^{-1}]	10.8 ± 0.2	7.05 ± 0.05	4.40 ± 0.2	2.60 ± 0.02
Loss (experiment) [dB cm^{-1}]	11.3 ± 0.1	7.30 ± 0.1	5.40 ± 0.1	3.00 ± 0.10

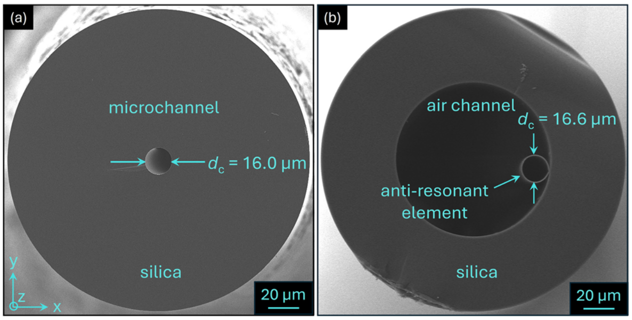

Fig. 6 Scanning electron micrographs (SEMs) of the fibers used in the FaNTA experiments: (a) capillary with a circular cross-section and a channel diameter of d_c = 16 µm, and (b) 1-ARE fiber featuring a partially suspended annular channel with a diameter of d_c = 16.6 µm.

cross-section, while also being well suited for tracking dielectric particles.

The experimental setup (Fig. 3) was identical to that used for the loss measurements, with adjusted image acquisition parameters (frame rate 450 fps and exposure time 1.95 ms). The optical power was kept sufficiently low (≈40 mW in case of the capillary) in order to prevent any light-induced heating effects.[13] Accurate determination of trajectories and hydrodynamic diameters requires aberration-free imaging to minimize localization errors – a key challenge in NTA generally (details on the effects of misalignment, see sec. S8 of the SI). Details regarding the effects of the frame rate, observation time, exposure time, and nanoparticle concentration are included in the SI, sec. S5.

Fig. 7 shows the distribution of hydrodynamic diameters from eight consecutive measurements (colored dots), determined *via* MSD analysis for both fiber types (top row: 1-ARE fiber, bottom row: capillary; benchmark values in Table 2). Note that the number of detected trajectories exceeds the actual number of NPs, due to intersecting trajectories or temporary loss of visibility when particles approach the channel wall and shows reduced scattering intensity. To ensure statistical significance, only trajectories

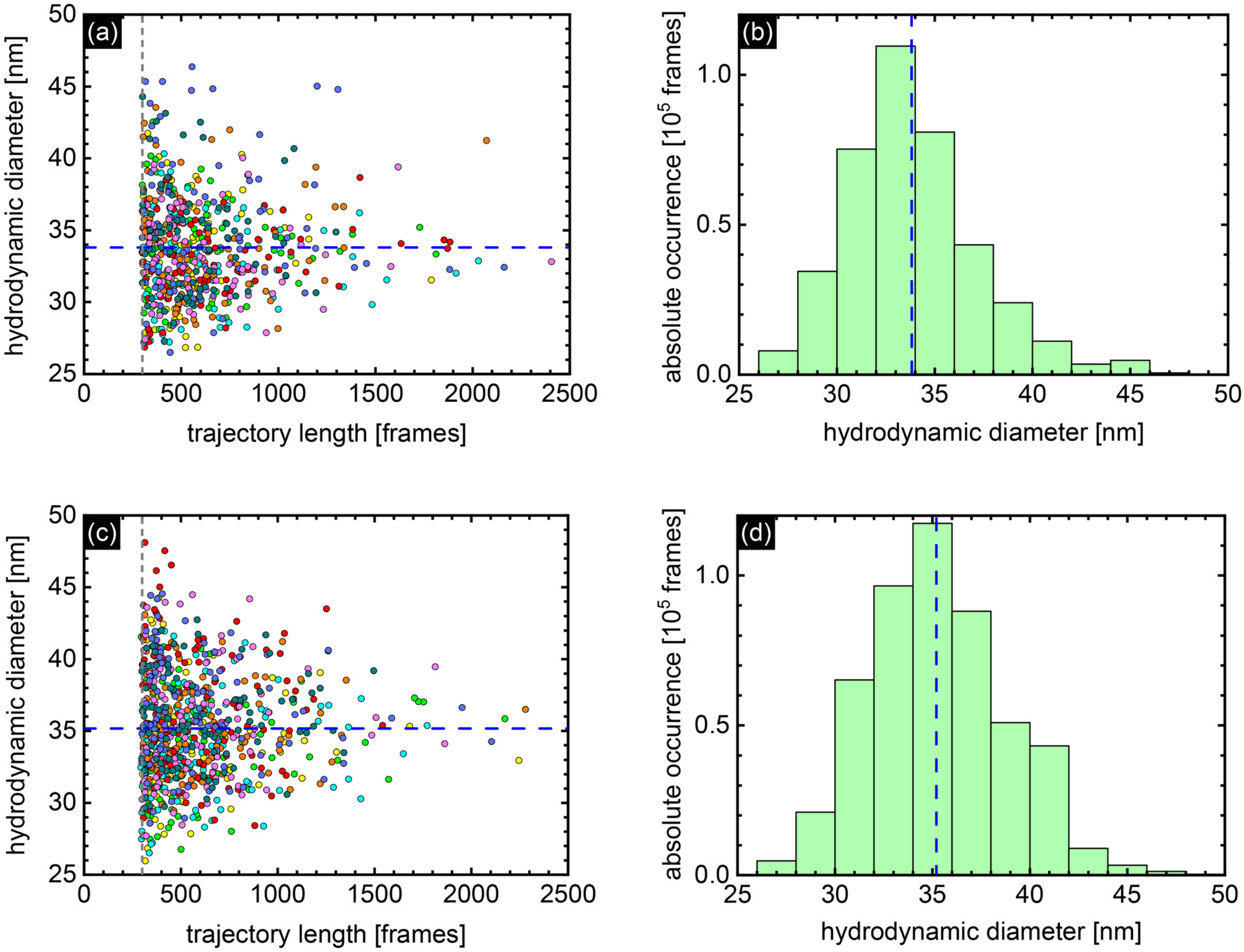

Fig. 7 Distribution of the hydrodynamic diameter for an ensemble of gold nanoparticles with an average physical diameter of 28 nm, measured using a 1-ARE fiber (top row) and a capillary (bottom row). (a) and (c) Hydrodynamic diameter as a function of trajectory length for eight consecutive measurements, each shown in a different color. The vertical gray dashed line indicates the minimum number of frames (300) required for a trajectory to be included in the analysis. (b) and (d) Corresponding weighted histograms. In all four plots, the blue dashed lines mark the mean hydrodynamic diameter.

Table 2 Comparison between NTA results and manufacturer specifications, showing the mean hydrodynamic diameters and coefficient of variation values determined using the capillary and the 1-ARE-fiber

Measurement method	Mean hydrodynamic diameter [nm]	CV	Standard deviation of the distribution [nm]
DLS (manufacturer)	36	Not specified	Not specified
FaNTA with 1-ARE-fiber	33.8 ± 0.7	0.093 ± 0.014	3.1 ± 0.5
FaNTA with capillary	35.3 ± 0.9	0.095 ± 0.010	3.4 ± 0.4

with a minimum length of 300 frames were included in the analysis (vertical dashed grey lines in Fig. 7(a and c).

The experiments demonstrate that the mean hydrodynamic diameters (blue dashed lines in Fig. 7) obtained from both fiber-based systems closely match each other and agree well with DLS reference measurements (Table 2), confirming the suitability of capillaries as a platform for NTA.

The strong agreement between the two FaNTA results is particularly noteworthy, given that two different NP ensembles were measured. The slightly smaller diameters observed in the FaNTA experiments compared to DLS may be attributed to the approximately 2300-fold dilution of the NP stock solution required for FaNTA, which could have led to partial detachment of PEG ligands from the NP surface. Comparable CV values for both fiber types further support the reliability and applicability of the capillary-based FaNTA approach.

Polydisperse mixture of polystyrene nanoparticles. To demonstrate the applicability of the capillary system for analyzing polydisperse NP mixtures, measurements were performed on a 1 : 1 mixture of polystyrene NPs (Thermo Fisher Scientific Inc.) with physical diameters of (100 ± 4) nm (specie 3100A) and (122 ± 3) nm (specie 3125A). Experimental details including measurements of monodisperse solutions are provided in sec. S9 of the SI. Note that this mixture consists of the same particle types that were used in our previous work (M. Nissen *et al.*[12] addressing FaNTA in a 1-ARE fiber.

As shown in Fig. 8, the capillary-based approach enables a clear distinction between the two NP populations in terms of their hydrodynamic diameters. Notably, some particles exhibit trajectory lengths of up to 11 000 frames, indicating that they remained trackable over 27.5 s, representing an exceptionally long observation time in the context of NTA.

As summarized in Table 3, the hydrodynamic diameters obtained for the NP mixture are in very good agreement with those measured for the corresponding monodisperse samples. In addition, the observation that the particle solution with the larger nominal diameter (3125A) exhibits a slightly narrower diameter distribution (lower CV value) is confirmed by our FaNTA measurements and is consistent with the manufacturer's TEM specifications. The results are also in good agreement with those reported by M. Nissen *et al.*[12]

Cluster formation of functionalized gold nanoparticles. To demonstrate the capability of the capillary-based FaNTA approach to characterize cluster formation, core–shell-type poly(*N*-isopropylacrylamide) (P*N*iPAAm)-functionalized gold NPs exhibiting thermo-responsive clustering behavior depending on the ionic strength of the solution[24,25] were investigated. These surface-grafted macromolecules possess a

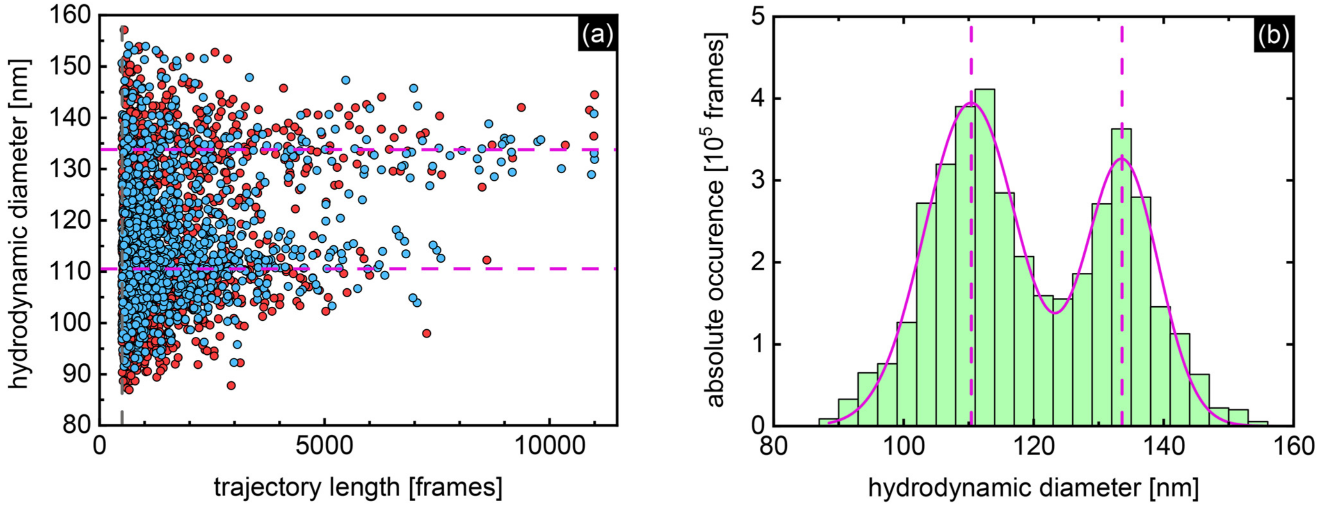

Fig. 8 Results of NTA measurements on a 1 : 1 mixture of 100 nm and 122 nm polystyrene NPs using a capillary with an inner diameter of 20.2 μm: (a) hydrodynamic diameter as a function of trajectory length for two independently analyzed ensembles of the mentioned mixture (ensemble 1: red dots; ensemble 2: blue dots), each comprising eight consecutive measurements. (b) Corresponding histogrammic representation of the hydrodynamic diameter distribution including a bimodal Gaussian fit. In both plots, the purble dashed lines indicate the mean hydrodynamic diameter of the respective distributions. In Fig. 8(a) the vertical dashed gray line indicates the minimum number of frames included in the analysis.

Table 3 Results of the FaNTA measurements obtained with the capillary-based FaNTA platform (this work) and the 1-ARE fiber (data taken from M. Nissen *et al.*[12]) for the two monodisperse polystyrene NP samples and their 1 : 1 mixture. Note that in the DLS measurements the two components in the mixture measurements could not be resolved; therefore, no mean hydrodynamic diameters can be reported for the mixed sample

		Monodisperse sample		NP mixture	
Measurement method	Parameter	3100A	3125A	3100A	3125A
FaNTA, capillary [this work]	Mean hydr. diam. [nm]	110.3 ± 0.2	132.8 ± 0.3	110.4 ± 0.3	133.6 ± 0.4
	CV [%]	5.9	5.7	6.5	4.2
FaNTA, 1-ARE [Nissen *et al.*]	Mean hydr. diam. [nm]	107.9 ± 0.1	132.8 ± 0.3	111.3	134.3
DLS [Nissen *et al.*]	Mean hydr. diam. [nm]	108.7 ± 0.5	131.4 ± 0.8	N.A.	N.A.

lower critical solution temperature (LCST) of approximately 32 °C at normal pressure. Above this temperature, the polymer chains undergo an intra-chain coil-to-globule transition,[26] which in this case results in a reduction of the hydrodynamic diameter from approximately 60 nm to about 37 nm.[27]

With a collapsed polymer shell, this type of NPs remain colloidally stable at low ionic strength due to electrostatic stabilization. In the case of high ionic strength achieved by adding electrolytes, electrostatic screening reduces interparticle repulsion and induces NP clustering.[24,25] Details of the sample preparation and the thermo-responsive behavior are provided in sec. S10 of the SI.

Fig. 9(b) shows the trajectory-length-weighted histograms in case a precise amount of electrolytes are added to the NP solution: At lower temperature (green), the distribution exhibits a narrow, single-peak profile centered around approximately 60 nm. This reflects the hydrated, expanded coil state of the polymer shell below the LCST, where the NPs remain well dispersed. In contrast, at elevated temperature (red), the distribution shifts significantly toward larger hydrodynamic diameters and broadens markedly. The appearance of particles with diameters extending beyond 150 nm clearly indicates temperature-induced cluster formation. The pronounced broadening of the distribution demonstrates the transition from a predominantly monodisperse suspension to a polydisperse ensemble of aggregates upon heating above the LCST. Thus, supracolloidal assembly processes induced by external stimuli can be effectively captured and resolved using capillary-based FaNTA.

Imaging considerations. In NTA, accurately determining the position of NPs within the water-filled channel of the used measurement fiber requires aberration-free imaging through the cladding. To evaluate the image quality of our microscopic concept, we performed simulations using the ray-tracing software Zemax Optics Studio (version v22.1.1), in order to determine the point spread function (PSF) and ray distribution (spot diagram Fig. 10) in the image plane for different transverse positions (*xy*-plane) of a light-emitting NP inside the water-filled channel (see sec. S7 of the SI for more details).

From the spot diagrams in Fig. 10(b and c), it is evident that for NPs positioned in the focal plane (center of the capillary channel), all rays fall within the airy disk diameter, confirming diffraction-limited imaging (an overview of the key performance indicators can be found in Table 4). This is supported by the small RMS (root mean square) value of the ray distribution (≈5.2 μm), which is well below the airy disk

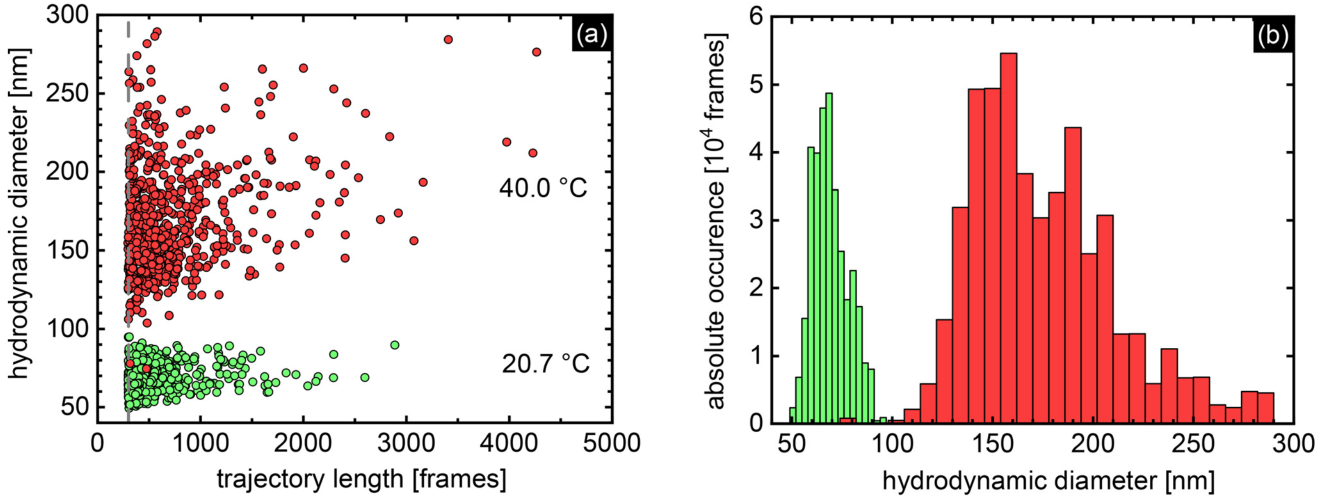

Fig. 9 Temperature-induced cluster formation of P*Ni*PAAm-functionalized gold nanoparticles (physical diameter 27 nm) in case the temperature is increased from 20.7 °C to 40 °C. (a) Hydrodynamic diameters of the NP ensemble as a function of trajectory length at *T* = 20.7 °C (green) and *T* = 40 °C (red). (b) Corresponding trajectory-length-weighted histograms of the hydrodynamic diameter distributions at *T* = 20.7 °C (green) and *T* = 40 °C (red). The *z*-score filtering (see sec. S4 of the SI) was not used to determine the diameter distribution of the cluster formation.

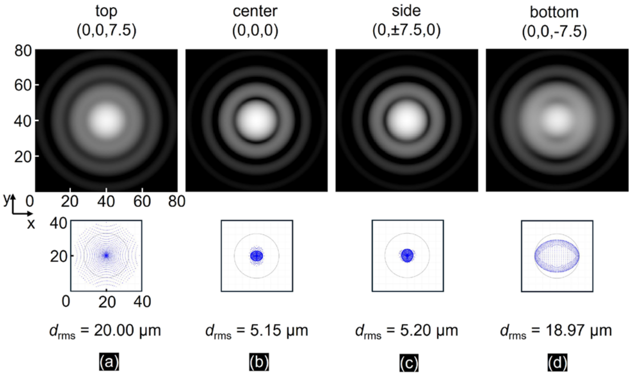

Fig. 10 Results of the ray-tracing simulations for four positions (top: (a), center: (b), side: (c), and bottom: (d)) of a light-emitting NP inside the water-filled channel (16 μm diameter) of the capillary (see Fig. S2(b) of the SI, sec. S7). The top row shows the PSF (logarithmic gray scale, representing 3 orders of magnitude) in the image plane ((80 × 80) μm after 10× magnification) for the imaging system focused on the channel center (axis). The bottom row shows the corresponding spot diagram in the image plane (40 × 40) μm, where each dot represents a single ray hitting the image plane. The traced rays uniformly fill the objective aperture (NA = 0.25) with square distribution. The black circle marks the airy disk, indicating the diffraction-limited diameter (d_{Airy} = $M{\cdot}1.22\ \lambda/NA$). The values d_{rms} indicate the RMS diameter of all calculated rays. The imaging system is considered diffraction-limited if the RMS diameter is smaller than the airy disk diameter of ≈26 μm in the image plane for the optical system used (≈2.6 μm in the object plane).

diameter (26 μm). Particles outside the focal plane (Fig. 10(a and d)) show a broadened distribution, as evident in Fig. 10(a) for the top position, where the particle is located 7.5 μm from the focal plane (0.5 μm from the capillary wall). Although some rays extend beyond the airy disk diameter, the RMS value remains below it, confirming diffraction-limited imaging even in this scenario. These findings demonstrate that the configuration investigated here maintains diffraction-limited optical resolution with negligible aberrations. The primary effect observed is minor defocusing at the top and bottom positions, which does not affect tracking since NP positions are determined by fitting the scattered light intensity profile to locate the centroid. Simulations also reveal that for capillaries with inner diameters greater than 20 μm, the RMS value for NP located more than 7.5 μm from the focal plane may exceed the airy disk diameter, resulting in imaging that is no longer diffraction-limited (see Table 4).

2.4 Discussion

As the results show, capillaries represent a promising alternative to 1-ARE fibers for NTA measurements. Despite their significantly lower structural complexity, they yield comparable benchmark figures, particularly in terms of imaging properties. Their overall suitability depends on optical losses and the signal-to-noise ratio (ratio of scattering intensity between nanoparticle and liquid). For instance, at a channel diameter of d_c = 20 μm, losses in capillaries are over an order of magnitude higher compared to 1-ARE fibers.[12] These elevated dissipative losses stem from lateral light leakage and result in a higher background scattering signal.

Based on the signal-to-noise ratio of the measurement on 28 nm gold NPs and the corresponding scattering cross-section (27 nm^2), we estimate the smallest detectable diameter of gold NPs, using a capillary, to be approximately 15 nm. Results of the experimental verification of this estimate are presented in the SI, sec. S11.

The experiments showed that this requires the use of capillaries with larger inner diameter (*e.g.* a 25 μm capillary with $\gamma \approx 2.6$ dB cm^{-1}), detection as close as possible to the capillary input, and a laser power of at least 130 mW at the capillary input.

Unlike gold nanoparticles, dielectric particles have a significantly smaller scattering cross-section due to their lower refractive index contrast and the absence of plasmon resonances, resulting in a larger minimum detectable diameter. In case of polystyrene NPs ($n_D \approx 1.6$) in water, this corresponds to a diameter limit of about 40 nm. Detection of smaller NPs requires 1-ARE fibers, which offer lower loss and higher SNR, enabling characterization of gold NPs down to 9 nm,[13] albeit requiring a substantially higher structural complexity of the waveguide used.

Importantly, the smallest detectable NP diameter in FaNTA is fundamentally limited by the Rayleigh scattering background of water. Consequently, increasing the excitation power to enhance weak scattering signals also raises the background, making the detection of small NPs challenging.

Note that the FaNTA approach generally enables accurate characterization of NPs with dimensions well below the

Table 4 Results of the ray tracing simulations, showing the RMS-diameter of the spot distribution [μm] for the capillary and 1-ARE fiber after 10× magnification. The positions indicated in the table header correspond to the positions shown in Fig. S2 (in sec. S7 of the SI) for a channel diameter of 16 μm or 25 μm. Images with RMS-diameter values below 26 μm can be considered as diffraction limited. Definition of the coordinate system: *x* – along the channel, *y* – cross the channel, *z* – cross the channel and along the optical axis of the imaging system

	Position	Top	Center	Side	Bottom
Type of fiber	(*x*, *y*, *z*) [μm]	(0, 0, 7.5)	(0, 0, 0)	(0, ±7.5, 0)	(0, 0, −7.5)
Capillary (16 μm)		20.00	5.15	5.20	18.97
1-ARE fiber (16 μm)		20.71	4.64	4.69	20.33
	(*x*, *y*, *z*) [μm]	(0, 0, 12)	(0, 0, 0)	(0, ±12, 0)	(0, 0, −12)
Capillary (25 μm)		31.42	5.27	5.46	29.65
1-ARE fiber (25 μm)		32.44	4.70	4.79	31.72

wavelength of light, whereas larger particles are challenging to analyze in the context of NTA due to hydrodynamic hindrance, sedimentation, dominant forward light scattering, reduced localization accuracy, and aberrations. Details are provided in sec. S12 of the SI.

As demonstrated capillary-based NTA provides a streamlined platform for the characterization of nanoscale particles in liquid environments. In the context of the present study, its primary capability lies in the accurate determination of hydrodynamic diameters and size distributions of mono- and polydisperse NP ensembles, which enables a wide range of applications. In nanoscience, it enables real-time monitoring of the growth dynamics of individual NPs with high spatial and temporal resolution. In life sciences, the approach is particularly attractive as a non-destructive method for the characterization of nanoscale biological objects, such as viruses or vesicles.

Here previous FaNTA studies have demonstrated the analysis of SARS-CoV-2 viruses,[28] cowpea chlorotic mottle viruses,[8] and bacteriophages (T4-phages,[29] Lambda-phages[11]), with high precision and long tracking durations, highlighting the capability of FaNTA for unlabeled viral particles in the size range of a few tens to a few hundred nanometers.

In addition to bioanalytics, further prospective applications include monitoring the NP content in industrial fluids,[30,31] detecting and characterizing nanoscale contaminants in water samples[32] and pharmaceutical products.

The capillary-based FaNTA approach is in principle transferable to other liquid media, as demonstrated, for example, for the 1-ARE fiber in a nanorheology study.[22] Note that reliable application requires careful consideration of the medium viscosity and sufficient signal-to-noise ratio, which depends on adequate refractive index contrast between the particle and the surrounding liquid.[33] Overall, the structural simplicity, robustness, and fiber compatibility of the capillary approach make it a promising tool for routine characterization of nano-objects across disciplines.

In contrast to scanning electron microscopy and transmission electron microscopy, FaNTA enables analysis of nano-objects in their native fluidic environment and does not require particle immobilization, which can potentially alter NP properties and interactions.

Even though the presented NTA experiments were conducted under static conditions, the capillary platform is inherently compatible with microfluidic operation schemes. Stopped-flow configurations can be readily realized by sequential introduction of defined particle ensembles into the observation region,[34,35] and NP tracking under low, well-controlled flow conditions at different Peclet numbers is feasible by incorporating drift-correction.[36] Thus, while the present study focuses on methodological validation in a stationary regime, the capillary platform offers a solid foundation for future integration into flow-based lab-on-a-chip architectures, which is the subject of a future study.

The added value of the capillary-based FaNTA approach in a microfluidic context arises from its intrinsic waveguide-based excitation directly within the liquid-filled channel, its compact fiber-compatible geometry, the extremely small sample volume required, and the fully enclosed configuration. Together, these features enable straightforward integration into micro- and optofluidic architectures while maintaining controlled measurement conditions.

3 Conclusion

In summary, we have demonstrated that fiber-type capillaries can be effectively used for waveguide-based nanoparticle tracking analysis, enabling precise characterization of mono- and polydisperse nanoparticle ensembles with accuracy comparable to more complex microstructured fiber platforms, like 1-ARE fibers. Our study quantitatively validates optical losses in water-filled capillaries, showing excellent agreement between experiment and theory.

The primary application demonstrated in this work is the reliable determination of hydrodynamic diameters and size distributions of various nanoscale species under different scenarios in aqueous environments. Specifically, we demonstrate the capillary system's ability to resolve monodisperse ensembles and polydisperse nanoparticle mixtures, as well as monitor the formation of temperature-induced clusters of functionalized nanoparticles. Additionally, we defined the upper operational limit for the largest nanoparticle size and experimentally verified the smallest diameter of nanoparticles that can be determined with this system.

Optical simulations and experimental results confirm diffraction-limited imaging performance, supporting reliable particle tracking in a streamlined geometry.

While the present study primarily concentrates on the methodological validation and benchmarking against established fiber platforms in the context of FaNTA, the capillary-based approach may serve as a foundation for future investigations of nanoparticle behavior in confined geometries. Owing to its structural simplicity, robustness, and fiber compatibility, the system is well suited for potential integration into microfluidic environments. In the future, this technology may find applications in fields such as nanoscience, bioanalytics, and environmental monitoring. Overall, the capillary platform provides a streamlined and accessible implementation of FaNTA for nanoscale particle characterization within the experimentally validated parameter range.

Author contributions

T. W.: measurement setup, experiments, data evaluation, theoretical calculations, writing – original draft; W. H.: ray tracing simulations; M. Z.: theory; A. L.: fiber production; S. V. L.: sample preparation; C. R.: conceptualization, writing – original draft; M.A.S.: funding acquisition, conceptualization, writing – original draft. All authors have accepted responsibility for the entire content of this manuscript and approved its submission.

Conflicts of interest

There are no conflicts to declare.

Data availability

Raw data from the nanoparticle tracking experiments and data from the ray tracing simulations using Zemax can be found in https://doi.org/10.5281/zenodo.17192038.

Supplementary information (SI) is available. See DOI: https://doi.org/10.1039/d6lc00339g.

Acknowledgements

The authors thank the team of the IPHT Fiber Competence Center for the manufacturing of the special hollow core fiber as well as IPHT Competence Center for Micro and Nano Technology for SEM images. Ruosong Wang is acknowledged for preparing the 27 nm citrate-capped gold nanoparticles. The authors acknowledge support by the German Research Foundation (DFG) *via* the projects 512648189 and SCHM2655/15-1 and the Open Access Publication Fund of the Thueringer Universitaets- und Landesbibliothek Jena.

References

1 H. Xie, Y. Yang, C. Xia, T.-C. Lee, Q. Pu, Y. Lan and Y. Zhang, *TrAC, Trends Anal. Chem.*, 2022, **146**(1–9), 116508.
2 R. P. B. Jacquat, G. Krainer, Q. A. E. Peter, A. N. Babar, O. Vanderpoorten, C. K. Xu, T. J. Welsh, C. F. Kaminski, U. F. Keyser, J. J. Baumberg and T. P. J. Knowles, *Nano Lett.*, 2023, **23**, 1629–1636.
3 L. Yu, Y. Lei, Y. Ma, M. Liu, J. Zheng, D. Dan and P. Gao, *Front. Phys.*, 2021, **9**, 1–21.
4 J. Stetefeld, S. A. McKenna and T. R. Patel, *Biophys. Rev.*, 2016, **8**, 409–427.
5 N. S. Ginsberg, C.-L. Hsieh, P. Kukura, M. Piliarik and V. Sandoghdar, *Nat. Rev. Methods Primers*, 2025, **5**, 1–21.
6 M. R. Moser and C. A. Baker, *Anal. Methods*, 2021, **13**, 2357–2373.
7 J. Gouyon, A. Boudier, F. Barakat, A. Pallotta and I. Clarot, *Electrophoresis*, 2022, **43**, 2377–2391.
8 S. Faez, Y. Lahini, S. Weidlich, R. F. Garmann, K. Wondraczek, M. Zeisberger, M. A. Schmidt, M. Orrit and V. N. Manoharan, *ACS Nano*, 2015, **9**, 12349–12357.
9 S. Jiang, J. Zhao, R. Förster, S. Weidlich, M. Plidschun, J. Kobelke, R. F. Ando and M. A. Schmidt, *Nanoscale*, 2020, **12**, 3146–3156.
10 F. Gui, S. Jiang, R. Förster, M. Plidschun, S. Weidlich, J. Zhao and M. A. Schmidt, *Adv. Photonics Res.*, 2021, **2**(1–9), 2100032.
11 R. Förster, S. Weidlich, M. Nissen, T. Wieduwilt, J. Kobelke, A. M. Goldfain, T. K. Chiang, R. F. Garmann, V. N. Manoharan, Y. Lahini and M. A. Schmidt, *ACS Sens.*, 2020, **5**, 879–886.
12 M. Nissen, R. Förster, T. Wieduwilt, A. Lorenz, S. Jiang, W. Hauswald and M. A. Schmidt, *Small*, 2022, **18**(1–10), 2202024.
13 T. Wieduwilt, R. Förster, M. Nissen, J. Kobelke and M. A. Schmidt, *Nat. Commun.*, 2023, **14**(1–7), 3247.
14 J. Kim, R. Förster, T. Wieduwilt, B. Jang, J. Bürger, J. Gargiulo, L. de S. Menezes, C. Rossner, A. Fery, S. A. Maier and M. A. Schmidt, *ACS Sens.*, 2022, **7**, 2951–2959.
15 D. Pereira, T. Wieduwilt, W. Hauswald, M. Zeisberger, M. S. Ferreira and M. A. Schmidt, *Light: Sci. Appl.*, 2025, **14**, 1–14.
16 P. Dress, M. Belz, K.-F. Klein, K. T. V. Grattan and H. Franke, *Sens. Actuators, B*, 1998, **51**, 278–284.
17 E. A. J. Marcatili and R. A. Schmeltzer, *Bell Syst. Tech. J.*, 1964, **43**, 1783–1809.
18 M. Zeisberger and M. A. Schmidt, *Sci. Rep.*, 2017, **7**(1–13), 11761.
19 M. Daimon and A. Masumura, *Appl. Opt.*, 2007, **46**, 3811–3820.
20 I. H. Malitson, *J. Opt. Soc. Am.*, 1965, **55**, 1205–1209.
21 J. R. Coe and T. B. Godfrey, *J. Appl. Phys.*, 1944, **15**, 625–626.
22 T. Wieduwilt, H. Geißler, R. Förster, A. Lorenz and M. A. Schmidt, *Nanophotonics*, 2025, **14**, 935–945.
23 https://www.malvernpanalytical.com/en/learn/knowledge-center/insights/polydispersity-what-does-it-mean-for-dls-and-chromatography.
24 S. ichi Yusa, K. Fukuda, T. Yamamoto, Y. Iwasaki, A. Watanabe, K. Akiyoshi and Y. Morishima, *Langmuir*, 2007, **23**, 12842–12848.
25 V. A. Turek, S. Cormier, B. Sierra-Martin, U. F. Keyser, T. Ding and J. J. Baumberg, *Adv. Opt. Mater.*, 2018, **6**, 1–6.
26 C. M. Papadakis, B.-J. Niebuur and A. Schulte, *Langmuir*, 2024, **40**, 1–20.
27 C. Rossner, I. Letofsky-Papst, A. Fery, A. Lederer and G. Kothleitner, *Langmuir*, 2018, **34**, 8622–8628.
28 R. Förster, T. Wieduwilt, M. Nissen and M. A. Schmidt, *2021 Conference on Lasers and Electro-Optics (CLEO)*, San Jose, CA, USA, 2021, pp. 1–2.
29 M. Nissen, *PhD thesis*, FSU Jena, Jena, Germany, 2025.
30 A. L. Rocca, G. D. Liberto, P. J. Shayler, C. D. J. Parmenter and M. W. Fay, *Tribol. Int.*, 2014, **70**, 142–147.
31 V. M. Rodriguez-DeVecchis, L. C. Ortega, C. E. Scott and P. Pereira-Almao, *Ind. Eng. Chem. Res.*, 2015, **54**, 9877–9886.
32 C. Jiang, S. Liu, T. Zhang, Q. Liu, P. J. J. Alvarez and W. Chen, *Environ. Sci. Technol.*, 2022, **56**, 7426–7447.
33 C. F. Bohren and D. R. Huffman, *Absorption and Scattering of Light by Small Particles*, WILEY-VCH Verlag GmbH Co, KGaA, 1998.
34 M. A. Levenstein, C. Chevallard, F. Malloggi, F. Testard and O. Taché, *Lab Chip*, 2025, **25**, 1169–1227.
35 D. Dendukuri, S. S. Gu, D. C. Pregibon, T. A. Hattona and P. S. Doyle, *Lab Chip*, 2007, **7**, 818–828.
36 https://soft-matter.github.io/trackpy/v0.7/.